High magnetic susceptibility of fault gouge within Taiwan Chelungpu fault: Nondestructive continuous measurements of physical and chemical properties in fault rocks recovered from Hole B, TCDP

Tetsuro Hirono,[1] Weiren Lin,[1] En-Chao Yeh,[1] Wonn Soh,[1] Yoshitaka Hashimoto,[2] Hiroki Sone,[3] Osamu Matsubayashi,[4] Kan Aoike,[5] Hisao Ito,[5] Masataka Kinoshita,[6] Masafumi Murayama,[7] Sheng-Rong Song,[8] Kuo-Fong Ma,[9] Jih-Hao Hung,[9] Chien-Ying Wang,[9] and Yi-Ben Tsai[9]

Received 4 March 2006; revised 12 June 2006; accepted 21 June 2006; published 3 August 2006.

[1] The Taiwan Chelungpu-fault Drilling Project (TCDP) was undertaken in 2002 to investigate the faulting mechanism of the 1999 Taiwan Chi-Chi earthquake. Hole B penetrated the Chelungpu fault, and recovered core samples from between 948.42 m and 1352.60 m depth. Three zones, marked 1136mFZ, 1194mFZ and 1243mFZ, were recognized in the core samples as active fault-zones within the Chelungpu fault. Multi-Sensor Core Logger measurements revealed lower densities and higher magnetic susceptibilities within the black gouge zones in all three fault zones. Even though the fault zone that slipped during the 1999 earthquake has not been identified, higher magnetic susceptibilities indicate that frictional heating has taken place in the Chelungpu fault. **Citation:** Hirono, T., et al. (2006), High magnetic susceptibility of fault gouge within Taiwan Chelungpu fault: Nondestructive continuous measurements of physical and chemical properties in fault rocks recovered from Hole B, TCDP, *Geophys. Res. Lett.*, *33*, L15303, doi:10.1029/2006GL026133.

1. Introduction

[2] The Chi-Chi earthquake (M_w7.6) on 21 September 1999 was the largest inland earthquake in Taiwan in the 20th century. The earthquake occurred at 23.853°N and 120.816°E with a focal depth of 8 km [*Ma et al.*, 1999] (Figure 1). The earthquake was initiated from a hypocenter in the southern Chelungpu fault and ruptured both upward and laterally northward [*Chen et al.*, 2001; *Ma et al.*, 2000]. It was well recorded by a dense seismic observatory network (Taiwan Strong Motion Network) operated by the Central Weather Bureau [*Shin et al.*, 2000]. The stations near the northern end of the Chelungpu fault recorded the largest ground velocities and displacements, 4.5 m/s and 12 m, respectively. In contrast, ground accelerations were higher in the southern part of the fault, even though the ground velocities and fault displacements were less than in the north. *Andrews* [2005] proposed that differences in the effect of thermal pressurization, combined with the differences in lithology of units within the fault zones in the north and south, explained these contrasting slips.

[3] Another notable contrast in slip behaviors was the marked absence of high-frequency radiations recorded in the near-field seismograms at the northern part of the fault. *Ma et al.* [2003] explained this by considering the slipping mechanism of elasto-hydrodynamic lubrication, assuming the presence of viscous fluidized fault gouge within the fault zone. It is suggested that the increased lubrication pressure widened the fault gap, thereby reducing the areas of asperity in contact and decreasing high-frequency radiations.

[4] As both thermal pressurization and hydrodynamic lubrication are appealing hypotheses, we attempt to explore their viability through analyses of rock samples of the fault-zones. Suitable samples were collected in the Taiwan Chelungpu-fault Drilling Project (TCDP) that started in 2002, with two cored holes, Hole A (depth 2003.00 m) and Hole B (depth 1352.60 m). In Hole B, cores were recovered from between 948.42 m and 1352.60 m, and the cores were analyzed in the Kochi Institute (JAMSTEC) by nondestructive continuous measurements. In this paper, we report on the occurrence of fault-zones that belong to the Chelungpu fault in Hole B core samples, and present the density, magnetic susceptibility and natural gamma ray characteristics of core samples from within these fault zones.

2. Description of the Chelungpu Fault

[5] The Chelungpu fault is developed within the Chinshui Shale, and its strike and dip are roughly parallel to those of the shale bedding plane (Figure 1). The underlying Sanyi fault separates the Keuichulin and Cholan Formations. These motions are of thrust type, and represent the second westernmost zone of deep thrusting of in the Taiwan mountain belt.

[6] Hole B penetrated the Cholan Formation, Chinshui Shale, and the Keuichulin Formation (Figure 1). We found

[1]Kochi Institute for Core Sample Research, Japan Agency for Marine-Earth Science and Technology, Nankoku, Japan.
[2]Department of Natural Environmental Science, Faculty of Science, Kochi University, Kochi, Japan.
[3]Department of Geology and Mineralogy, Graduate School of Science, Kyoto University, Kyoto, Japan.
[4]Institute for Geo-Resources and Environment, National Institute of Advanced Industrial Science and Technology, Tsukuba, Japan.
[5]Center for Deep Earth Exploration, Japan Agency for Marine-Earth Science and Technology, Yokohama, Japan.
[6]Institute for Research on Earth Evolution, Japan Agency for Marine-Earth Science and Technology, Yokosuka, Japan.
[7]Center for Advanced Marine Core Research, Kochi University, Kochi, Japan.
[8]Department of Geosciences, National Taiwan University, Taipei, Taiwan.
[9]Institute of Geophysics, National Central University, Jhongli, Taiwan.

0094-8276/06/2006GL026133$05.00

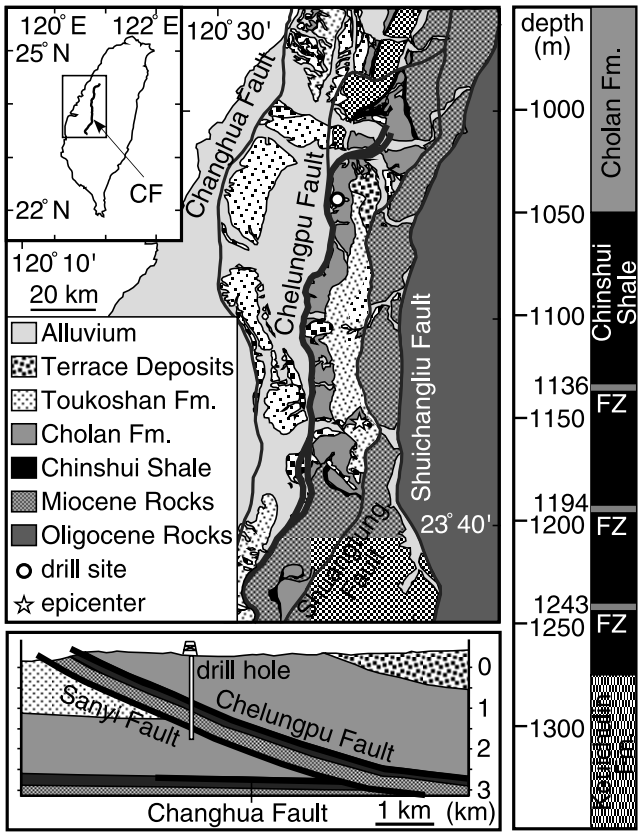

Figure 1. Geological map of central Taiwan, showing the site of the Taiwan Chelungpu-fault Drilling Project (TCDP), an E-W cross section through the site location, and the lithogical column of core samples recovered from Hole B. CF: Chelungpu Fault, FZ: fault zone.

evidence of the Chelungpu fault in core samples recovered from Hole B, where three dominant fault zones were recognized. These zones were at depths of 1134–1137 m, 1194–1197 m, and 1242–1244 m, and we named them 1136mFZ, 1194mFZ, and 1243mFZ, respectively.

[7] A core recovery rate of almost 100% was achieved, and the core diameter was 83 mm. The fault rocks were classified into fracture-damaged zone, fault breccia (breccia zone), and fault gouge, which terminology was followed by *Sibson* [1977] and *Biegel and Sammis* [2004].

[8] The following subdivisions were encountered, from top to bottom, in 1136mFZ (Figure 2): upper fracture-damaged zone (1134.40–1134.93 m), upper breccia zone (1134.93–1136.22 m), upper gray fault gouge (1136.22–1136.26 m), black fault gouge (1136.26–1136.40 m), lower gray fault gouge (1136.40–1136.46 m), lower breccia zone (1136.46–1136.70 m), and lower fracture-damaged zone (1136.70–1137.90 m). Both fracture-damaged zones displayed layer-parallel and subparallel open-fractures, which were sparsely developed in an alternation of sandstones and mudstone with bioturbation. In both breccia zones, the clasts were fine-grained sandstone with minor shear bands, and the foliations within the matrixes became more intense closer to the gouge zone. Both gouge zones displayed foliation or random fabric, and were separated by a graduated boundary.

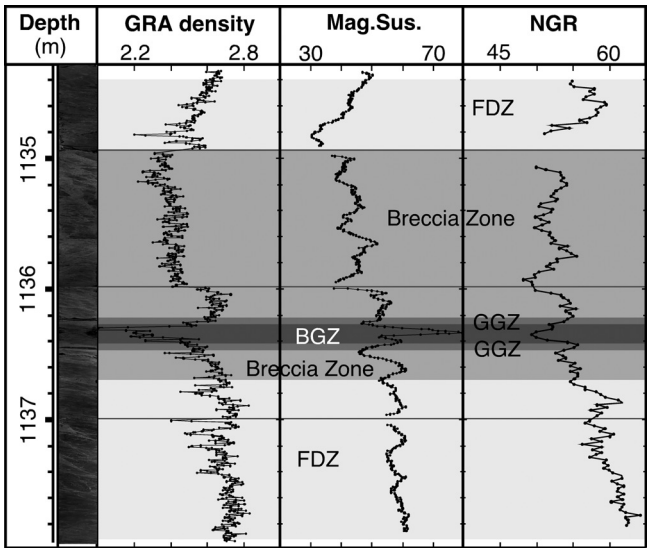

Figure 2. Density, magnetic susceptibility (Mag.Sus.) and natural gamma ray radiation (NGR) logs from 1136mFZ. The units are g/cm^3, 10^{-5}SI, and cps, respectively. FDZ: fracture-damaged zone, BGZ: black gouge zone, GGZ: gray gouge zone.

[9] In 1194mFZ, subdivisions observed from top to bottom were (Figure 3): upper fracture-damaged zone (1194.00–1194.73 m), black fault gouge (1194.73–1194.87 m), gray fault gouge (1194.87–1195.13 m), breccia zone (1195.13–1195.50 m), and lower fracture-damaged zone (1195.50–1197.25 m). The upper sandstone unit included minor shear bands. The black fault gouge included disk-shaped black material (1194.73–1194.75 m), which we have named BM disk. It was 2 cm in thickness, and relatively stiff compared with the gouge. The upper boundary was extremely sharp, whereas some fragments of the disk were contained in the underlying black gouge. Other parts of both gouge zones displayed foliation or random

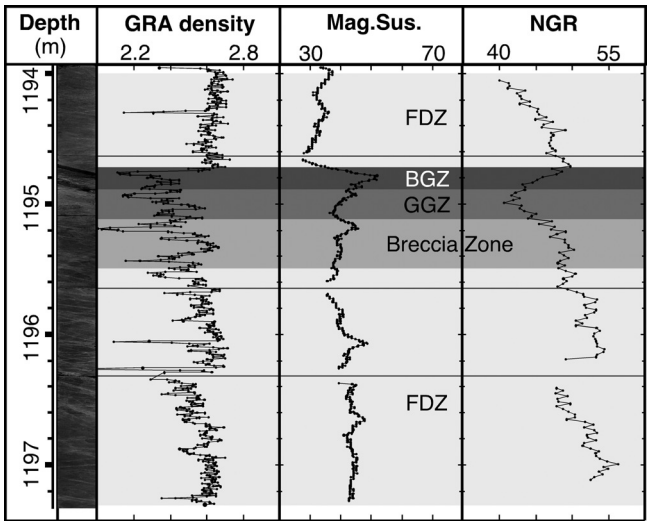

Figure 3. Density, magnetic susceptibility (Mag.Sus) and natural gamma ray radiation (NGR) logs from 1194mFZ. The units are g/cm^3, 10^{-5}SI, and cps, respectively. The abbreviations are the same to those in Figure 2.

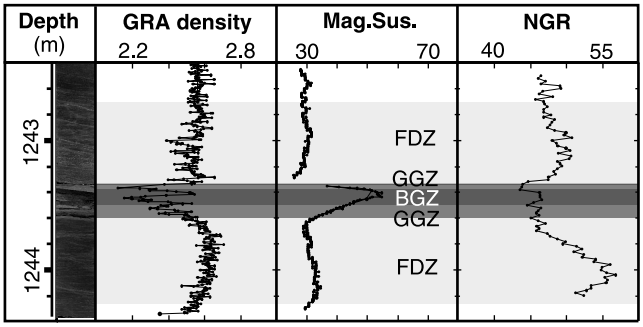

Figure 4. Density, magnetic susceptibility (Mag.Sus.) and natural gamma ray radiation (NGR) logs from 1243mFZ. The units are g/cm^3, 10^{-5}SI, and cps, respectively. The abbreviations are the same to those in Figure 2.

fabric. The breccia and fracture-damaged zones displayed similar to those in 1136mFZ.

[10] In 1243mFZ, subdivisions observed from top to bottom were (Figure 4): upper fracture-damaged zone (1242.70–1243.33 m), upper gray fault gouge (1243.33–1243.38 m), black fault gouge (1243.38–1243.50 m), lower gray fault gouge (1243.50–1243.60 m), and lower fracture-damaged zone (1143.60–1244.30 m). The black fault gouge included disk-shaped black material (1243.38–1243.41 m). It was 3 cm in thickness, and relatively stiff compared with the gouge, similar to that encountered in 1194mFZ. Other parts of both gouge zones displayed foliation or random fabric. The fracture-damaged zones displayed similar to those in other two fault zones.

[11] The architectures of 1136mFZ was characterized as symmetric while both of1194mFZ and 1243mFZ were asymmetric with the BM disk layers.

3. Hole B Core Measurements

[12] The nondestructive continuous measurements were conducted using the Multi-Sensor Core Logger (MSCL) system as described below. Photo images were also captured using the logger.

3.1. Gamma Ray Attenuation (GRA) Density

[13] Bulk density of sample materials was determined by measuring the attenuation of gamma rays passed through the cores, which is based on the principle that the level of attenuation, due mainly to Compton scattering, is proportional to the density of the tested material. The thin gamma ray beam is provided by a 137-Cs gamma ray source at a radiation level of 370 Bq within a lead shield with a 2.5-mm collimator, and the detector comprises a scintillator and an integral photomultiplier tube. Calibration is achieved using a standard piece comprising a stepwise machined cylindrical aluminum piece and distilled water. The error of the GRA density is lower than 0.01 g/cm^3. GRA measurement was conducted every 0.5 cm for a period of 4 s.

3.2. Magnetic Susceptibility

[14] Magnetic susceptibility is the degree to which material can be magnetized by an external magnetic field. The Bartington loop sensor (MS2C) with a 10-cm loop diameter was used for magnetic susceptibility measurements. An oscillator circuit in the sensor produces a low intensity (approx. 80 A/m RMS) non-saturating, alternating magnetic field (0.565 kHz). Any material that has a magnetic susceptibility will, in the near vicinity of the sensor, cause a change in the oscillator frequency. This pulse frequency is converted into magnetic susceptibility values. The spatial resolution of the loop sensor is 20–30 mm, and it is accurate to within less than 2%. The data was determined at an interval of 0.5 cm with 4-s acquisition times using a 1.0-s integration time range.

3.3. Natural Gamma Radiation (NGR)

[15] NGR system records radioactive decay of ^{40}K, ^{232}Th, and ^{238}U, which are three long-period isotopes that decay at an essentially constant rate within measurable time scales. A lead-shielded counter was used, which was optically coupled to a photomultiplier tube and connected to a bias base that supplied the high voltage power and a signal pre-amplifier. Two sensors were mounted horizontally in a lead cube housing. Background radiation intensity of 38 cps was measured by inserting a blank piece filled with quartz powder. The spatial resolution was 150 mm, and the accuracy of measured data was within about 1.5%. The NGR was measured every 2 cm for a 2-minute period.

4. Results

[16] The GRA density, magnetic susceptibility, and NGR data obtained from three dominant fault zones are summarized in Figure 2 (1136mFZ), Figure 3 (1194mFZ), and Figure 4 (1243mFZ). In all the fault zones, the GRA densities were mostly in the range from 2.0 to 2.8 g/cm^3, but showed significantly lower values within the black gouge zones. The magnetic susceptibilities fluctuated mainly from 28×10^{-5} to 60×10^{-5} SI, but also showed higher peak values within the black gouge zones. The NGR emissions ranged from 40 to 68 cps, and showed lower values weakly correlated with the gouge zones.

[17] As for lower GRA densities in the black gouge zones in all three fault zones, they collapsed at the outer edges of the cores and some portions were washed out, because they were relatively fragile. Therefore, the total volume of the samples analyzed for these parts of the sequence may have been less than elsewhere. However, the sediment thickness was measured by the MSCL, and was used for calibration and to calculate density. Thus, the lower densities recorded in the black gouge zones could not be explained as the decreasing of thickness. Conversely, the lower values could result from real densities, possibly caused by more extensive fracturing in this part of the sequence. Porosities, measured by TDR moisture probe, were higher within the black gouge zones (Lin, personal communication 2006). These data support fracturing as the cause, rather than washout effects.

[18] Across the fault zones, magnetic susceptibilities only in 1136mFZ increased with depth, and the NGR emissions in all the fault zones appeared to increase in the footwalls. These fluctuations might result from lithological changes of original host rocks.

5. Discussion

[19] We think that the measured magnetic susceptibility in the cores provides some indications on the nature of the slip mechanism during the earthquake. The magnetic susceptibility of a rock is strongly influenced by the

concentration of ferrimagnetic minerals such as magnetite and hematite, and also by the grain size of those ferrimagnetic minerals [e.g., *Dearing*, 1999]. There are two possible explanations for the high magnetic susceptibility of the black gouge: (1) ferrimagnetic grains were crushed into submicron size by shearing, while the total concentration of magnetic mineral did not change; (2) magnetite or maghemite grains were newly formed by thermal decomposition of paramagnetic phases such as siderite [*Pan et al.*, 2000] and lepidocrosite [*Özdemir and Dunlop*, 1993].

[20] Mesoscopic examinations of the black gouge zones within all three fault zones showed intense shear fabric, indicating that they could be classified as cataclasite or ultracataclasite. This supports the hypothesis that grain-size reduction was responsible for the high magnetic susceptibilities. However, although the gray fault zones also showed intense shear fabrics, their magnetic susceptibilities were not relatively higher. Thus, grain-size reduction was not necessarily responsible.

[21] On the other hand, clay mineral analyses within a fault zone in Hole A [*Kuo et al.*, 2005] suggested a thermal history including temperature of more than 450°C, which is consistent with the hypothesis that frictional heating was responsible for the high magnetic susceptibilities recorded. *Fukuchi et al.* [2005] undertook the high-speed frictional testing of natural fault gouge, and demonstrated the production of ferrimagnetic iron oxides as a result of thermal dehydration induced by frictional heating of antiferrimagnetic iron oxides. Thus, it can be concluded that temperature rise by frictional heating was more responsible rather than grain-size reduction.

[22] Numerical analyses of measured physical properties of fault-zone rocks [*Noda and Shimamoto*, 2005] have illustrated that the temperature rise within a fault zone is controlled by the rate of heat production, which strongly depends on the evolution of fault shear strength due to thermal pressurization. Weaker effect of thermal pressurization leads to much frictional heating and a temperature rise. *Sone et al.* [2005] conducted similar numerical analyses on the Chelungpu fault using the data obtained from Hole-A. Their results also showed weaker effect of thermal pressurization leads to rapid temperature rise. Thus, if such black gouge zone has a thermal history above a certain level, it may imply the limited effectiveness of thermal pressurization that may have taken place within the three fault zones in the Chelungpu fault.

6. Summary

[23] Hole B penetrated the Chelungpu fault, and core samples were recovered from depths ranging from 948.42 m to 1352.60 m. Three-fault zones, 1136mFZ, 1194mFZ and 1243mFZ, were recognized in the core samples as series within the Chelungpu fault. Each of the fault zones included black fault gouge, and, in particular, 1194mFZ and 1243mFZ also included disk-shaped black material within the black gouge zones. MSCL measurements revealed lower GRA densities and higher magnetic susceptibilities within the black gouge zones. Even though the fault zone that slipped during the 1999 earthquake has not been identified, high magnetic susceptibilities measured within all three fault zones reveal that they have all experienced frictional heating. Advanced measurement techniques, such as magnetic mineral analyses, may provide further information of temperature experienced that is important for gaining an understanding of the lubrication mechanism within faults during the 1999 Chi-Chi earthquake.

References

Andrews, D. J. (2005), Thermal pressurization explains enhanced long-period motion in the Chi-Chi earthquake, *Eos Trans. AGU*, *86*(52), Fall Meet. Suppl., Abstract S34A-04.

Biegel, R. L., and C. G. Sammis (2004), Relating fault mechanics to fault zone structure, *Adv. Geophys.*, *47*, 65–111.

Chen, K. C., B. S. Huang, J. H. Wang, W. G. Huang, T. M. Chang, R. D. Hwang, H. C. Chiu, and C. C. P. Tsai (2001), An observation of rupture pulses of the 20 September 1999 Chi-Chi, Taiwan, earthquake from near-field seismograms, *Bull. Seismol. Soc. Am.*, *91*, 1247–1254.

Dearing, J. (1999), Magnetic susceptibility, in *Environmental Magnetism: A Practical Guide*, edited by J. Walden, F. Oldfield, and J. Smith, Quat. Res. Assoc., London, 35–62.

Fukuchi, T., K. Mizoguchi, and T. Shimamoto (2005), Ferrimagnetic resonance signal produced by frictional heating: A new indicator of paleoseismicity, *J. Geophys. Res.*, *110*, B12404, doi:10.1029/2004JB003485.

Kuo, L., S. Song, and H. Chen (2005), Characteristics of clay minerals in the fault zone of TCDP and its implications, *Eos Trans. AGU*, *86*(52), Fall Meet. Suppl., Abstract T43D-05.

Ma, K. F., C. T. Lee, Y. B. Tsai, T. C. Shin, and J. Mori (1999), The Chi-Chi Taiwan earthquake: Large surface displacements on inland thrust fault, *Eos Trans. AGU*, *80*(50), 605, 611.

Ma, K. F., T. R. Song, S. J. Lee, and S. I. Wu (2000), Spatial slip distribution of the September 20, 1999, Chi-Chi Taiwan earthquake: Inverted from teleseismic data, *Geophys. Res. Lett.*, *27*, 3417–3420.

Ma, K. F., E. E. Brodsky, J. Mori, C. J. T. R. A. Song, and H. Kanamori (2003), Evidence for fault lubrication during the 1999 Chi-Chi, Taiwan, earthquake (*Mw*7.6), *Geophys. Res. Lett.*, *30*(5), 1244, doi:10.1029/2002GL015380.

Noda, H., and T. Shimamoto (2005), Thermal pressurization and slip-weakening distance of a fault: An example of the Hanaore Fault, southwest Japan, *Bull. Seismol. Soc. Am.*, *95*, 1224–1233.

Özdemir, O., and D. J. Dunlop (1993), Chemical remanent magnetization during γFeOOH phase transformations, *J. Geophys. Res.*, *98*, 4191–4198.

Pan, Y. X., R. X. Zhu, S. K. Banerjee, J. Gill, and Q. Williams (2000), Rock magnetic properties related to thermal treatment of siderite: Behavior and interpretation, *J. Geophys. Res.*, *105*, 783–794.

Shin, T. C., K. W. Kuo, W. H. K. Lee, T. L. Teng, and Y. B. Tsai (2000), A preliminary report on the 1999 Chi-Chi (Taiwan) earthquake, *Seismol. Res. Lett.*, *71*, 24–30.

Sibson, R. H. (1977), Fault rocks and fault mechanisms, *J. Geol. Soc. London*, *133*, 191–213.

Sone, H., T. Shimamoto, H. Noda, S. Song, K. Ma, J. Hung, and C. Wang (2005), Frictional properties and permeability of fault rocks from Taiwan Chelungpu-fault Drilling Project and their implications for high-velocity slip weakening, *Eos Trans. AGU*, *86*(52), Fall Meet. Suppl., Abstract T43D-06.

K. Aoike and H. Ito, Center for Deep Earth Exploration, Japan Agency for Marine-Earth Science and Technology, 3173-25 Showa-machi, kanazawa-ku, Yokohama, 236-0001, Japan.

Y. Hashimoto, Department of Natural Environmental Science, Faculty of Science, Kochi University, 2-5-1 Akebono-cho, Kochi 780-8520, Japan.

T. Hirono, W. Lin, W. Soh, and E.-C. Yeh, Kochi Institute for Core Sample Research, Japan Agency for Marine-Earth Science and Technology, Nankoku 783-8502, Japan. (hirono@jamstec.go.jp)

J.-H. Hung, K.-F. Ma, Y.-B. Tsai, and C.-Y. Wang, Institute of Geophysics, National Central University, Jhongda Road, Jhongli 32001, Taiwan.

M. Kinoshita, Institute for Research on Earth Evolution, Japan Agency for Marine-Earth Science and Technology, 2-15 Natsushima-cho, Yokosuka-shi, 237-0061, Japan.

O. Matsubayashi, Institute for Geo-Resources and Environment, National Institute of Advanced Industrial Science and Technology, Tsukuba, 305-8567, Japan.

M. Murayama, Center for Advanced Marine Core Research, Kochi University, 2-5-1 Akebono-cho, Kochi 780-8520, Japan.

H. Sone, Department of Geology and Mineralogy, Graduate School of Science, Kyoto University, Yoshida-Honmachi, Sakyo-ku, Kyoto 606-8501, Japan.

S.-R. Song, Department of Geosciences, National Taiwan University, Roosevelt Road, Taipei, Taiwan 106.